11. P. J. Godowski, S. Rusconi, R. Miesfeld, K. R. Yamamoto, *Nature* (*London*) **325**, 365 (1987).
12. S. Rusconi and K. R. Yamamoto, *EMBO J.*, in press.
13. V. Giguère, S. M. Hollenberg, M. G. Rosenfeld, R. M. Evans, *Cell* **46**, 645 (1986).
14. J. R. Grove, B. S. Dieckmann, T. A. Schroer, G. M. Ringold, *ibid.* **21**, 47 (1980).
15. G. M. Ringold *et al.*, *Proc. Natl. Acad. Sci. U. S.A.* **76**, 665 (1979).
16. K. R. Yamamoto, U. Gehring, M. R. Stampfer, C. H. Sibley, *Recent Prog. Horm. Res.* **32**, 3 (1976).
17. H. Baumann *et al.*, *J. Biol. Chem.* **258**, 563 (1983); R. Reinke and P. Feigelson, *ibid.* **260**, 4397 (1985).
18. G. M. Ringold, K. R. Yamamoto, G. M. Tomkins, J. M. Bishop, H. E. Varmus, *Cell* **6**, 299 (1975).
19. J. N. Vanderbilt, R. Miesfeld, B. A. Maler, K. R. Yamamoto, *Mol. Endocrinol.* **1**, 68 (1987).
20. J. Miller, A. D. MacLachlan, A. Klug, *EMBO J.* **4**, 1609 (1985).
21. R. T. Ogata and W. Gilbert, *J. Mol. Biol.* **132**, 709 (1979).
22. K. R. Yamamoto, *Annu. Rev. Genet.* **19**, 209 (1985).
23. M. Ptashne, *Nature* (*London*) **322**, 697 (1986).
24. A. Hochschild *et al.*, *Cell* **32**, 319 (1983); I. A. Hope and K. Struhl, *ibid.* **46**, 885 (1986); J. Ma and M. Ptashne, *ibid.* **48**, 847 (1987).
25. R. Miesfeld *et al.*, in *Sequence Specificity in Transcription and Translation*, vol. 30 of UCLA Symposium on Molecular and Cellular Biology, New Series, R. Calender and L. Gold, Eds. (Liss, New York, 1985), pp. 535–545; J. P. Northrop, B. Gametchu, R. W. Harrison, G. M. Ringold, *J. Biol. Chem.* **260**, 6398 (1985).
26. R. Miesfeld *et al.*, in *Steroid Hormone Action*, UCLA Symposium on Molecular and Cellular Biology, G. Ringold, Ed. (Liss, New York, in press).
27. M. Jacobson, R. Miesfeld, S. Rusconi, unpublished data.
28. S. A. Camper, Y. A. S. Yao, F. M. Rottman, *J. Biol. Chem.* **260**, 12246 (1985); J. H. Eberwine and J. L. Roberts, *ibid.* **259**, 2166 (1984).
29. K. R. Yamamoto, in *Molecular Developmental Biology: Expressing Foreign Genes*, 43rd Symposium of the Society for Developmental Biology, L. Bogorad and G. Adelman, Eds. (Liss, New York, 1985), pp. 131–148.
30. Receptor deletion mutants are denoted according to the following nomenclature: derivatives named with N or C contain receptor amino acids extending from the NH_2-terminus or COOH-terminus, respectively, through the given amino acid number (N795 is the intact receptor); derivatives denoted with an X begin at amino acid 407 and extend through the numbered amino acid; derivatives denoted by two hyphenated numbers include the receptor segment delineated by the given amino acid numbers; derivatives denoted with a Δ lack the receptor segment delineated by the numbered amino acids. Plasmids containing the intact receptor coding sequence, RBal117, RSVGR, and SVGR1, and the SV40 expression vector SV7d, have been described previously (*8*). Internal deletion derivatives Δ70–130 and Δ185–300 were constructed by cleavage of RBal117 DNA with Nco I and Bgl II, respectively, resection with exonuclease BAL31, attachment of Xho I linkers, and recircularization. In-frame fusions were identified by translation in vitro of transcripts produced with SP6 RNA polymerase; end points were estimated (±3 amino acids) by high-resolution gel electrophoresis. The mutant coding sequences were inserted into pRSVTG, the Rous sarcoma virus expression vector [H.-P. Moore and R. B. Kelly, *J. Cell. Biol.* **101**, 1773 (1985)] used to construct RSVGR. Internal deletion derivative Δ273–418 was constructed as an in-frame fusion of the Bgl II site to a Bam HI linker of a BAL31 terminal deletion, followed by insertion into SV7d. NH_2-terminal deletion derivatives were constructed by ligating Bam HI–linked BAL31 deletions to a BAM HI–linked herpes simplex virus (HSV) thymidine kinase leader sequence (*8*); in-frame fusions were identified by in vitro translation and characterized by DNA sequencing. All mutants were inserted into SV7d, except X795, which is expressed from a human α globin promoter/SV40 enhancer combination [S. Paabo, F. Weber, T. Nilsson, W. Schaffner, P. A. Peterson, *EMBO J.* **5**, 1921 (1986)]. Carboxyl-terminal BAL31 deletions were characterized by DNA sequencing and inserted into SV7d upstream of its triple termination codons, as described elsewhere (*8*, *12*). Double deletion derivatives (see Fig. 4) were constructed by fusing fragments from the respective mutant inserts upstream and downstream of the receptor Sph I site, followed by insertion into SV7d.
31. S. Rusconi and K. R. Yamamoto, unpublished data.
32. The MTV-infected rat hepatoma HTC cell derivatives M1.19 and 6.10.2 have been described (*8*, *14*, *15*); these lines, as well as the monkey COS-7 and CV-1 lines, were propagated in Dulbecco's modified Eagle's medium (Gibco) supplemented with 10% fetal bovine serum (Hyclone). The increased basal expression of MTV RNA observed in cell lines containing transfected receptor sequences (*8*) is eliminated by using fetal bovine serum rather than the defined calf serum used previously. Stable receptor transfectants were obtained by cotransfecting receptor sequences with a neomycin resistance marker, followed by G418 selection, isolation of cell clones, and characterization as described (*8*). Transient transfection of COS-7 and CV-1 cells was achieved by calcium phosphate precipitation of 5 μg of receptor expression plasmid together with 1 μg of the receptor-dependent CAT reporter plasmid GMCS (*8*); cultures were incubated in the presence or absence of 0.1 μM dexamethasone for 48 hours and cell extracts were assayed for CAT activity (*33*).
33. C. M. Gorman, L. F. Moffat, B. H. Howard, *Mol. Cell. Biol.* **2**, 1044 (1982).
34. We thank S. Rusconi for several of the mutant receptor inserts and for discussions. We thank R. Harrison for receptor-specific monoclonal antibodies; R. Grosschedl, D. Sakai, and P. Sternberg for comments; and K. Rañeses for manuscript preparation. This work was supported by grants from the National Science Foundation and the National Institutes of Health; postdoctoral fellowship support was from the Leukemia Society of America (R.M.) and NIH (P.J.G.); K.R.Y. is recipient of a teacher-scholar award from the Henry and Camille Dreyfus Foundation.

27 January 1987; accepted 19 March 1987

Ice-Edge Eddies in the Fram Strait Marginal Ice Zone

O. M. JOHANNESSEN, J. A. JOHANNESSEN, E. SVENDSEN, R. A. SHUCHMAN, W. J. CAMPBELL, E. JOSBERGER

Five prominent ice-edge eddies in Fram Strait on the scale of 30 to 40 kilometers were observed over deep water within 77°N to 79°N and 5°W to 3°E. The use of remote sensing, a satellite-tracked buoy, and in situ oceanographic measurements showed the presence of eddies with orbital speeds of 30 to 40 centimeters per second and lifetimes of at least 20 days. Ice ablation measurements made within one of these ice-ocean eddies indicated that melting, which proceeded at rates of 20 to 40 centimeters per day, is an important process in determining the ice-edge position. These studies give new insight on the formation, propagation, and dissipation of ice-edge eddies.

One objective of the Marginal Ice Zone Experiment (MIZEX-84) program is to better understand the physics of mesoscale eddies along an ice edge and the role that eddies play in the processes of mass and heat exchange and in controlling the position of the ice edge. Previous studies in the Fram Strait marginal ice zone (MIZ) have established the existence of mesoscale eddies at the ice edge with scales that range from 5 to 15 km north of Svalbard (*1*) to 50 to 60 km in the western parts of the Fram Strait (*2*). Barotropic and baroclinic instability mechanisms have been suggested as eddy-generating mechanisms. Since the topography of the central part of the Fram Strait is complex (with depressions of 4000 to 5500 m and seamounts up to 1400 m below the surface), topographic generation and trapping of eddies have also been suggested (*3*). A two-dimensional model (*4*) proposed an eddy generation mechanism that included differential wind-induced ice and ocean circulation. This report describes a dedicated eddy investigation during the summer of 1984 between 77°N and 79°N along the ice edge of Fram Strait. The study used remote sensing; conductivity, temperature, and depth (CTD) observations; and ice-drifting satellite-tracked buoys that were suspended with current meters.

Remote-sensing observations were used in a near real-time mode for locating eddies and for guiding the research vessels into the eddy region. For example, the high-resolution synthetic aperture radar (SAR) mosaic on 5 July (Fig. 1) clearly shows detailed surface structure of an elliptically shaped eddy E1 on the scale of ~30 km. Since the wind was light, the floe-size distribution of 50 to 500 m reflected the upper ocean circulation. The orbital motion was cyclonic, while the spiral motion of ice toward the center indicated frictionally driven inward radial motion. The ice concentration was more than 80% at the center of the eddy (see Fig. 1, A and B). This implied that there was convergence, and that ageostrophic effects are important and must be included in realistic models of these eddies. A second eddy

O. M. Johannessen, Geophysical Institute and Nansen Ocean and Remote Sensing Center, University of Bergen, Bergen, Norway.
J. A. Johannessen and E. Svendsen, Nansen Ocean and Remote Sensing Center, University of Bergen, Bergen, Norway.
R. A. Shuchman, Environmental Research Institute of Michigan, Ann Arbor, MI 48107.
W. J. Campbell and E. Josberger, U.S. Geological Survey, University of Puget Sound, Tacoma, WA 98416.

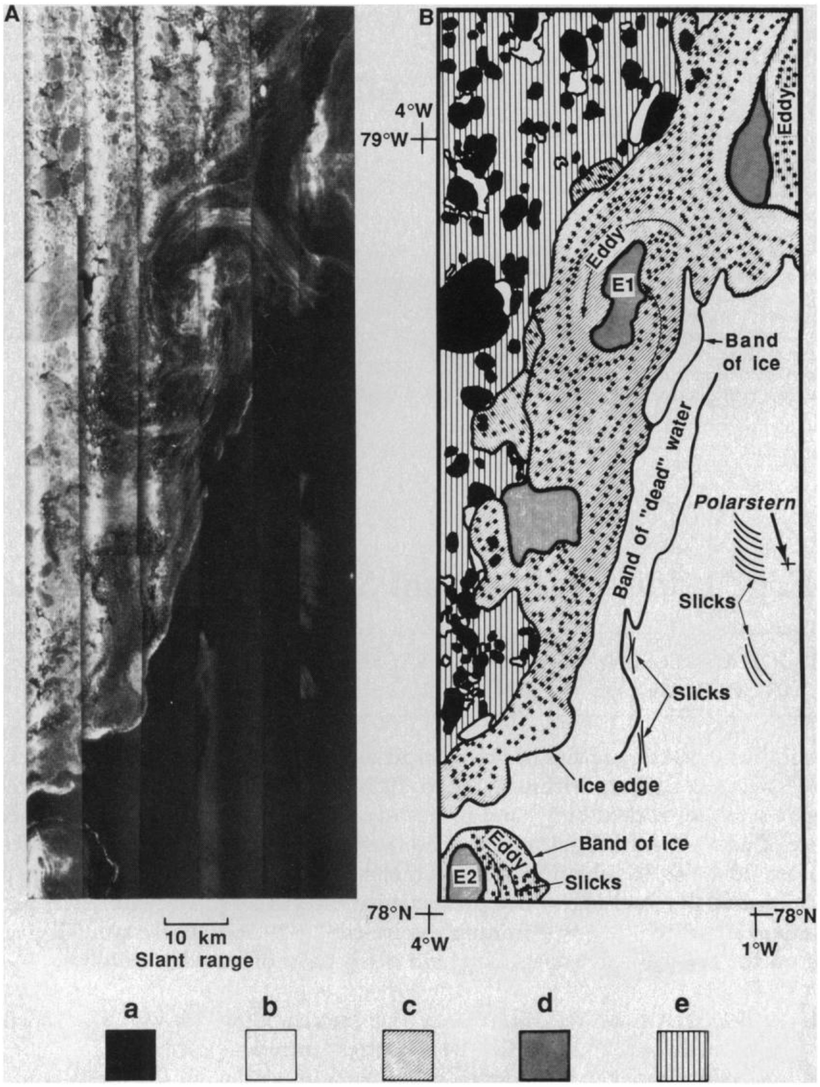

Fig. 1. (**A**) L-band (1.2 GHz) mosaic collected on 5 July 1984 with the X-C-L-band SAR system of the Environmental Research Institute of Michigan/Canadian Center of Remote Sensing. In the radar image bright zones represent ice and the dark zones are ice-free water. The large eddy E1 is clearly visible in the data at a resolution of 3 m by 3 m. (**B**) The interpretation of the SAR mosaic reveals that large individual floes (a), polynyas and ice-free ocean areas (b), 30% ice concentration areas with 10- to 500-m floes (c), 80% ice concentration areas with 10-m to 1.5-km floes (d), and 80% ice concentration areas with 10- to 6-km floes (e) are clearly delineated in the image. The median floe size for the areas marked c, d, and e is 125, 150, and 1000 m, respectively. The dots in (c) indicate increased local ice concentration due to surface currents.

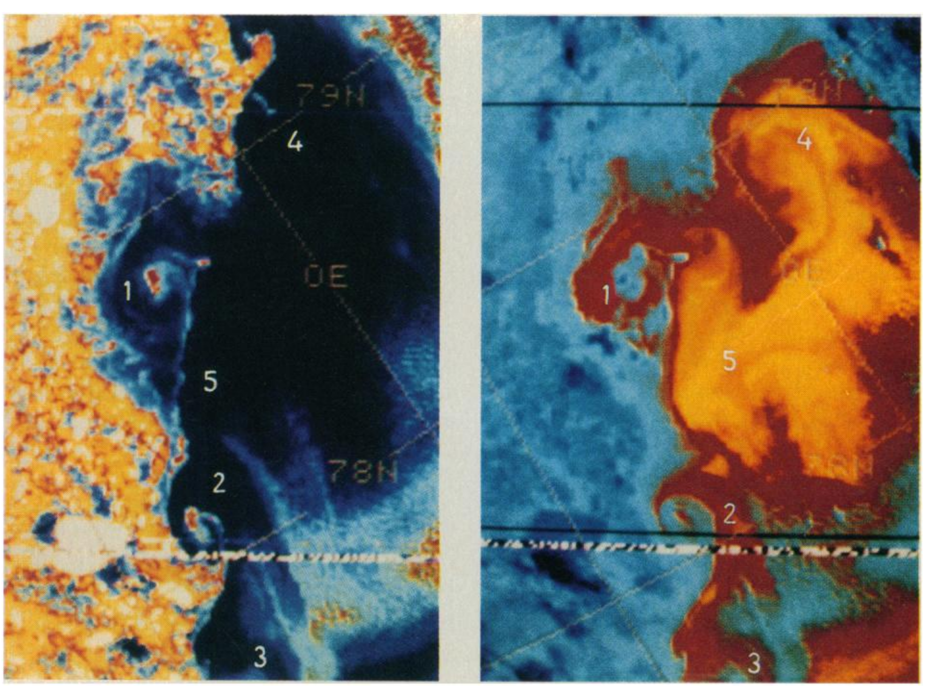

Fig. 2. NOAA-7 AVHRR image obtained on 4 July 1984. The left image is from the visible band, and the right image is simultaneously obtained from the infrared (IR) band. The resolution of both images is 1 km. Five eddies (numbered 1 through 5) are clearly observed in the IR image and three eddies can be distinguished in the visible band. In the IR image yellow is the warmest temperature (4°C), while red, light blue, and black (0°C) represent decreasing temperatures. [Image processed by K. Kloster, Christian Michelsens Institute, Bergen, Norway.]

E2 was seen south of E1 and was centered at 78°05′N and 3°55′W. Slicks and bands of ice were also identified that indicated internal wave activity. The area marked "Band of 'dead' water" off the ice edge was a distinct meltwater zone.

The abundance of eddies in this region (five overall) is shown in an image obtained with an advanced very high resolution radiometer (AVHRR) aboard the National Oceanic and Atmospheric Administration satellite NOAA-7 on 4 July (Fig. 2). Eddies E1 through E4 strongly interacted with the ice edge. Analyses of earlier AVHRR images showed that on 26 June E1 started to form at approximately 79°15′N and 1°30′W and was fully developed by 29 June at 79°N and 2°15′W. This suggested an upper layer spin-up time of the order of 3 days, during which time the mean southward advection of the eddy, deduced from these images, was approximately 10 km/day. From 30 June to 1 July E1 moved slowly eastward. The spin-up of E2, which was then 50 km southwest of E1, occurred during 1 to 4 July.

After 4 July, cloudiness precluded the continued use of the NOAA satellite for monitoring the eddies. However, aircraft microwave observations continued to provide high-resolution monitoring of the eddies and demonstrated that radar observations were indispensable for the experiment. Sequential radar images through 16 July showed that E1 was nearly stationary. A northerly wind (2 days' duration, 15 m/sec) erased the clear ice convergence signature within the eddy but did not completely erase the boundary signature, and demonstrated

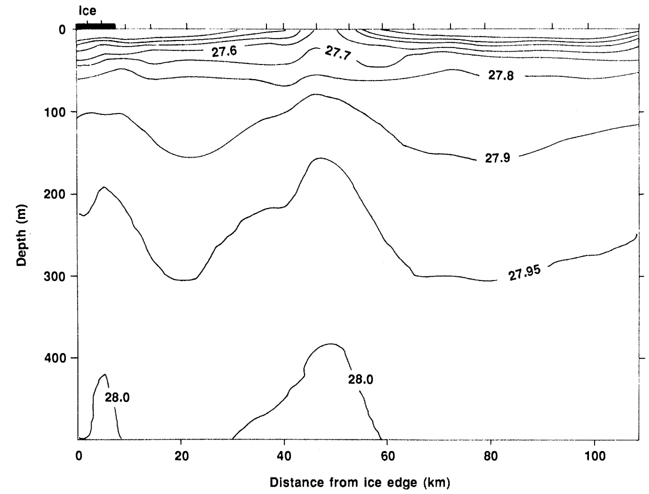

Fig. 3. Vertical density structure in the east-west direction perpendicular to the ice edge across eddy E1 near the center of the eddy. The units on the isopycnals are in $\Delta\rho t$.

that imaging radar can observe ice-ocean eddies even under high wind conditions. The ice convergence structure at the center reappeared when the wind decreased. The remote-sensing data showed that E1 had a lifetime of at least 20 days.

Extensive star pattern CTD sections of E1 obtained by the research vessels R.V. *Håkon Mosby* and R.V. *Kvitbjørn* during the period 10 to 14 July coupled with the remote-sensing observations during the same period give a nearly synoptic three-dimensional picture of the eddy. A section perpendicular to the ice edge (Fig. 3) near the center of E1 showed the doming and surfacing of the isopycnals, and indicated cyclonic motion down to 500 m and confirmed the rotation that was seen in the radar image. A CTD section in the north to south direction was obtained by R.V. *Polarstern* on 16 July and extended approximately 2500 m through to the bottom of E1. This section showed that E1 was actually present at depths of 800 to 1000 m. Measurements of current velocity within E1 (obtained by a satellite-tracked Argos buoy equipped with current meters) measured cyclonic orbital speeds of 30 to 40 cm/sec. The subsurface structures of E4 and E5 were also confirmed by CTD observations.

We could estimate the thermodynamic importance of eddies in determining the ice-edge position from the AVHRR image (Fig. 2). The cyclonic motion of each eddy not only swept ice away from the main ice pack but also transported warm Atlantic water (3° to 4°C) beneath the ice. Melt rates from the bottom of the ice tongue of E1 varied from 20 to 40 cm/day in contrast with rates of 2 to 3 cm/day when the ice was in the colder Arctic water. To estimate eddy thermodynamics, we assumed that half of the eddy was covered by ice and that the ice was 1.5 m thick; under such conditions the observed melt rates could easily account for the loss of approximately 350 km^2 of sea ice in 4 to 7 days. Hence at an eddy spacing of 50 km (Fig. 2), these eddies alone could cause the ice edge to melt at a rate of 1 to 2 km/day on average. Such intense melting was also observed from 1 to 6 June in the vicinity of the eddy E4 (*5*). The warming and thinning of the ice augmented by the eddies also made the ice more susceptible to fracturing by waves and floe collisions.

All of the eddies observed were cyclonic and were observed in an area of 3×10^5 km^2. They transferred heat from the warm Atlantic water to the ice and thus greatly enhanced the rates of ice melting. Eddies in the MIZ may play a more important role in transfer processes than eddies do in the temperate oceans. Both short- and long-forecasting models for range the ice edge position must include the effects of the eddies. Because of the close spacing of these eddies, our observations suggest that realistic MIZ models must include eddy-eddy interactions.

REFERENCES AND NOTES

1. O. M. Johannessen, J. A. Johannessen, J. Morison, B. Farrelly, E. Svendsen, *J. Geophys. Res.* **88**, 2755 (1983).
2. P. Wadhams and V. Squire, *ibid.*, p. 2770.
3. D. C. Smith, J. Morison, J. A. Johannessen, N. Untersteiner, *ibid.* **89**, 8205 (1984).
4. S. Hakkinen, thesis, Florida State University, Tallahassee (1984).
5. R. A. Shuchman *et al.*, *Science* **236**, 427 (1987).
6. This research was supported by the University of Bergen, the Royal Norwegian Council for Scientific and Industrial Research, the Norwegian Research Council for Science and Humanities, the U.S. Office of Naval Research (Arctic Programs), and the U.S. Geological Survey.

19 May 1986; accepted 14 January 1987

Remote Sensing of the Fram Strait Marginal Ice Zone

R. A. SHUCHMAN, B. A. BURNS, O. M. JOHANNESSEN,
E. G. JOSBERGER, W. J. CAMPBELL, T. O. MANLEY, N. LANNELONGUE

Sequential remote sensing images of the Fram Strait marginal ice zone played a key role in elucidating the complex interactions of the atmosphere, ocean, and sea ice. Analysis of a subset of these images covering a 1-week period provided quantitative data on the mesoscale ice morphology, including ice edge positions, ice concentrations, floe size distribution, and ice kinematics. The analysis showed that, under light to moderate wind conditions, the morphology of the marginal ice zone reflects the underlying ocean circulation. High-resolution radar observations showed the location and size of ocean eddies near the ice edge. Ice kinematics from sequential radar images revealed an ocean eddy beneath the interior pack ice that was verified by in situ oceanographic measurements.

A CENTRAL PROBLEM IN STUDIES OF the Fram Strait marginal ice zone (MIZ) is the definition of those mesoscale oceanic and atmospheric processes that determine the location of the ice edge, ice morphology, and ice deformation within the zone as well as the quantification of the major energy and momentum exchanges taking place there (*1*). Because marginal ice zones are located in regions that are either dark or cloudy for most of the year, microwave aircraft and satellite observations are the best means of obtaining high-resolution synoptic surface information. We present here an analysis of sequential high-resolution aircraft synthetic aperture radar (SAR) images from a region in the Fram Strait north of 79°N.

Figure 1 shows an SAR image obtained on 6 July 1984. This image, collected during total cloud cover from an altitude of 6.7 km,

R. A. Shuchman and B. A. Burns, Environmental Research Institute of Michigan, Ann Arbor, MI 48107.
O. M. Johannessen, Geophysical Institute–Nansen Ocean and Remote Sensing Center, University of Bergen, Bergen, Norway.
E. G. Josberger and W. J. Campbell, U.S. Geological Survey, Tacoma, WA 98416.
T. O. Manley, Lamont–Doherty Geological Observatory, Palisades, NY 10964.
N. Lannelongue, Centre National d'Études Spatiales, Toulouse, France.